

Calculations of N₂ triplet states vibrational populations and band emissions in Venusian dayglow

Anil Bhardwaj* and Sonal Kumar Jain†
 Space Physics Laboratory,
 Vikram Sarabhai Space Centre,
 Trivandrum, India - 695022

Abstract

A model for N₂ triplet states band emissions in the Venusian dayglow has been developed for low and high solar activity conditions. Steady state photoelectron fluxes and volume excitation rates for N₂ triplet states have been calculated using the Analytical Yield Spectra (AYS) technique. Model calculated photoelectron flux is in good agreement with Pioneer Venus Orbiter-observed electron flux. Since inter-state cascading is important for the triplet states of N₂, populations of different levels of N₂ triplet states are calculated under statistical equilibrium considering direct electron impact excitation, and cascading and quenching effects. Densities of all vibrational levels of each triplet state are calculated in the model. Height-integrated overhead intensities of N₂ triplet band emissions are calculated, the values for Vegard-Kaplan ($A^3\Sigma_u^+ - X^1\Sigma_g^+$), First Positive ($B^3\Pi_g - A^3\Sigma_u^+$), Second Positive ($C^3\Pi_u - B^3\Pi_g$), and Wu-Benesch ($W^3\Delta_u - B^3\Pi_g$) bands of N₂, are 1.9 (3.2), 3 (6), 0.4 (0.8), and 0.5 (1.1) kR, respectively, for solar minimum (maximum) conditions. The intensities of the three strong Vegard-Kaplan bands (0, 5), (0, 6), and (0, 7) are 94 (160), 120 (204), and 114 (194) R, respectively, for solar minimum (maximum) conditions. Limb profiles are calculated for VK (0, 4), (0, 5), (0, 6) and (0, 7) bands. The calculated intensities on Venus are about a factor 10 higher than those on Mars. The present study provides a motivation for a search of N₂ triplet band emissions in the dayglow of Venus.

1 Introduction

Ultraviolet (UV) emissions of Venus have been studied for decades by rocket-borne spectrometers, Mariner 10, Venera 11 and 12, and Galileo spacecraft flybys, Pioneer Venus Orbiter, and Hopkins Ultraviolet Telescope aboard Space Shuttle (e.g., [Fox and Bougher, 1991](#); [Paxton and Anderson, 1992](#); [Feldman et al., 2000](#); [Gérard et al., 2008](#)). More recently, Venusian UV emissions observed during the Cassini flyby have been reported ([Gérard et al., 2011](#); [Hubert et al., 2010](#)). The major UV emissions observed are from H, He, C, N, O and CO. However, until now the N₂ emissions have not been observed on Venus. Recently, SPICAM (Spectroscopy for Investigation of Characteristics of the Atmosphere of Mars) onboard Mars Express has observed, for the first time, emissions from N₂ triplet excited states. The main emissions observed are the (0, 6) and (0, 5) bands of the Vegard-Kaplan (VK) transitions of N₂ ([Leblanc et al., 2006](#),

[2007](#)). On Venus, the VK bands would be more intense compared to those on Mars because of its proximity to the Sun and higher N₂ abundances. SPICAV (Spectroscopy for Investigation of Characteristics of the Atmosphere of Venus) on Venus Express orbiter mission, which is similar to SPICAM, can able to observe these emissions in the Venusian dayglow.

We have recently developed a model for the N₂ triplet state dayglow emissions on Mars using the Analytical Yield Spectra approach ([Jain and Bhardwaj, 2011](#)). While calculating the emissions of triplet transitions of N₂, cascading from the higher lying states and quenching by atmospheric constituents are considered and the population of any given vibrational level of a state is calculated under statistical equilibrium. In the present paper, this model is used to calculate the N₂ dayglow emission on Venus for solar maximum and minimum conditions. Previous theoretical study on N₂ emissions in the Venusian dayglow

*anil_bhardwaj@vssc.gov.in; bhardwaj_spl@yahoo.com

†sonaljain.spl@gmail.com

have been carried out by [Fox and Dalgarno \(1981\)](#) and [Gronoff et al. \(2008\)](#). We compare our results with their model intensities.

2 Model Input Parameters

The model atmosphere considering five gases (CO₂, CO, N₂, O, and O₂) is taken from the VTS3 model of [Hedin et al. \(1983\)](#) for the low (F10.7 = 80) and high (F10.7 = 200) solar activity conditions. The EUVAC model of [Richards et al. \(1994\)](#) has been used to calculate the 37-bin solar EUV flux, which is based on the F10.7 solar index. The EUVAC solar spectrum is scaled for the heliocentric distance of Venus (0.72 AU). All calculations are made at solar zenith angle (SZA) of 60° unless otherwise noted. Photoionization and photoabsorption cross sections for gases considered in the present study have been taken from [Richards et al. \(1994\)](#) and [Schunk and Nagy \(2000\)](#). The branching ratios for excited states of CO₂⁺, CO⁺, N₂⁺, O⁺, and O₂⁺ have been taken from [Avakyan et al. \(1998\)](#). Franck-Condon factors and transition probabilities required for calculating the intensity of a specific band $\nu' - \nu''$ of N₂ are taken from [Gilmore et al. \(1992\)](#).

The electron impact N₂ triplet states excitation cross sections are taken from [Itikawa \(2006\)](#), which have been fitted analytically (cf. [Jackman et al., 1977](#); [Bhardwaj and Jain, 2009](#)) and fitting parameters are given in [Jain and Bhardwaj \(2011\)](#). Electron impact cross sections for CO₂ are from [Bhardwaj and Jain \(2009\)](#) and for other gases from [Jackman et al. \(1977\)](#).

3 Photoelectron Flux

To calculate the photoelectron flux we have adopted the Analytical Yield Spectra (AYS) technique (cf. [Bhardwaj et al., 1990](#); [Singhal and Bhardwaj, 1991](#); [Bhardwaj, 1999, 2003](#); [Bhardwaj and Michael, 1999](#)). The AYS is an analytical representation of numerical yield spectra obtained using the Monte Carlo model (cf. [Singhal et al., 1980](#); [Singhal and Bhardwaj, 1991](#); [Bhardwaj and Michael, 1999](#); [Bhardwaj and Jain, 2009](#)). Recently, the AYS model for electron degradation in CO₂ has been developed by [Bhardwaj and Jain \(2009\)](#). Further details of the AYS technique are given in [Bhardwaj and Jain \(2009\)](#) and references therein. Using AYS the photoelectron flux has been

calculated as

$$\phi(Z, E) = \int_{W_{kl}}^{100} \frac{Q(Z, E)U(E, E_0)}{\sum_l n_l(Z)\sigma_{lT}(E)} dE_0 \quad (1)$$

where $\sigma_{lT}(E)$ is the total inelastic cross section for the l th gas with density n_l , and $U(E, E_0)$ is the two-dimensional AYS, which embodies the non-spatial information of degradation process. It represents the equilibrium number of electrons per unit energy at an energy E resulting from the local energy degradation of an incident electron of energy E_0 . For the CO₂ gas it is given as ([Bhardwaj and Jain, 2009](#))

$$U(E, E_0) = A_1 E_k^s + A_2 (E_k^{1-t} / \epsilon^{3/2+r}) + \frac{E_0 B_0 e^x / B_1}{(1 + e^x)^2} \quad (2)$$

Here $E_k = E_0/1000$, $\epsilon = E/I$ (I is the lowest ionization threshold), and $x = (E - B_2)/B_1$. $A_1 = 0.027$, $A_2 = 1.20$, $t = 0$, $r = 0$, $s = -0.0536$, $B_0 = 10.095$, $B_1 = 5.5$, and $B_2 = 0.9$ are the best fit parameters.

For other gases, viz., O₂, N₂, O, and CO, we have used the AYS given by [Singhal et al. \(1980\)](#)

$$U(E, E_0) = C_0 + C_1(E_k + K)/[(E - M)^2 + L^2]. \quad (3)$$

Here C_0 , C_1 , K , M , and L are the fitted parameters which are independent of the energy, and whose values are given by [Singhal et al. \(1980\)](#). The term $Q(Z, E)$ in equation (1) is the primary photoelectron production rate (cf. [Michael and Bhardwaj, 1997](#); [Bhardwaj, 2003](#); [Jain and Bhardwaj, 2011](#)).

Model calculated photoelectron fluxes at 130, 150, and 250 km altitudes for solar minimum condition at SZA=60°, are shown in the upper panel of Figure 1. A sudden drop in flux at ~3 eV is due to the large vibrational cross sections at 3.8 eV for electron impact on CO₂ (cf. [Bhardwaj and Jain, 2009](#)). The sharp peak at 27 eV is due to ionization of CO₂ in the ground state by the He II solar Lyman α line at 303.78 Å. The broad peak at 21-23 eV is due to ionization of CO₂ in the A²Π_u and B²Σ_u⁺ states of CO₂⁺ by the 303.78 Å solar photons. Peak structures around 20-30 eV are clearly seen in the photoelectron flux at 150 km, whereas they are smoothed out at 130 km, indicating that solar He II Lyman α photons are largely degraded at higher altitudes and do not reach altitudes of 130 km. The calculated flux decreases exponentially with increasing energy. A sharp fall in the photoelectron flux at ~70 eV is due to the presence of this features in the primary photoelectron energy spectrum resulting

from photoionization process. (Jain and Bhardwaj, 2011).

Figure 1 (bottom panel) shows the calculated photoelectron fluxes for solar maximum condition (F10.7=200) at SZA=20°. Photoelectron flux features are similar to those in solar minimum conditions. This figure also shows the electron flux measured by the Pioneer Venus Orbiter Retarded Potential Analyser (Spenner et al., 1997). Good agreement both in shape and magnitude, is observed between the calculated and measured fluxes. Spenner et al. (1997) found that the average electron fluxes do not vary much for SZA between 0° and 70°.

4 Results and discussion

The volume excitation rate for N₂ emissions is calculated as

$$V_i(Z, E) = n(Z) \int_{E_{th}}^E \phi(Z, E) \sigma_i(E) dE, \quad (4)$$

where $n(Z)$ is the density of N₂ at altitude Z and $\sigma_i(E)$ is the electron impact cross section for the i th state, for which the threshold is E_{th} . Figure 2 shows the excitation rates of N₂ triplet states (A , B , C , W , B' , and E) by photoelectron impact excitation. During both solar minimum and maximum conditions, excitation rate for all the states peaks at ~135-140 km. However, at the peak, the excitation rates during solar maximum are a factor of 2 higher than that during solar minimum, while at higher altitudes (~200 km and above) the increase is by a factor of 5 or more.

All transitions between the triplet states of N₂ and the ground state are spin forbidden, therefore excitation of these states is primarily due to the electron impact. The higher lying states C , W , and B' populate the B level, which in turn radiate to the A level. Inter-system cascading $B^3\Pi_g \rightleftharpoons A^3\Sigma_u^+$ and $B^3\Pi_g \rightleftharpoons W^3\Delta_u$ are also important in populating the B level (Cartwright et al., 1971; Cartwright, 1978). All excitations to the higher triplet states eventually cascade into the $A^3\Sigma_u^+$ state (Cartwright et al., 1971; Cartwright, 1978). The effect of reverse first positive transition is important in populating the lower vibrational levels of the B state, which in turn populate the lower vibrational levels of the A state (Sharp, 1971; Cartwright et al., 1971; Cartwright, 1978). The width and shape of VK bands are quite sensitive to the rotational temperature, making it a useful tool

to monitor the neutral temperature of the upper atmosphere (Broadfoot et al., 1997). To calculate the contribution of cascading from higher triplet states and interstate cascading between different states, we solve the equations for statistical equilibrium based on the formulation of Cartwright (1978). At a specified altitude, for a vibrational level ν of a state α , the population is determined using the statistical equilibrium equation

$$V^\alpha q_{0\nu} + \sum_\beta \sum_s A_{s\nu}^{\beta\alpha} n_s^\beta = \{K_{q\nu}^\alpha + \sum_\gamma \sum_r A_{\nu r}^{\alpha\gamma}\} n_\nu^\alpha \quad (5)$$

where

V^α	electron impact volume excitation rate (cm ⁻³ s ⁻¹) of state α ;
$q_{0\nu}$	Franck-Condon factor for the excitation from ground level to ν level of state α ;
$A_{s\nu}^{\beta\alpha}$	transition probability (s ⁻¹) from state $\beta(s)$ to $\alpha(\nu)$;
$K_{q\nu}^\alpha$	total electronic quenching frequency (s ⁻¹) of level ν of state α by the all gases defined as: $\sum_l K_{q(l)\nu}^\alpha \times n_l$; where, $K_{q(l)\nu}^\alpha$ is the quenching rate coefficient of level ν of α by gas l of density n_l ;
$A_{\nu r}^{\alpha\gamma}$	transition from level ν of state α to vibrational level r of state γ ;
n	density (cm ⁻³);
α, β, γ	electronic states;
s, r	source and sink vibrational levels, respectively.

While calculating the cascading from C state, we have accounted for predissociation. The C state predissociates approximately half the time (this is an average value for all vibrational levels of the C state; excluding $\nu = 0, 1$, which do not predissociate at all) (cf. Daniell and Strickland, 1986). In Earth's airglow the N₂(A) levels get effectively quenched by atomic oxygen and the abundance of O increases with increase in altitude. In the case of Venus the main atmospheric constituent CO₂ does not quench the N₂(A) levels that efficiently because of much lower quenching rate coefficient for CO₂, but still there will be some collisional deactivation by other atmospheric constituents of Venus. The quenching rates for different vibrational levels of N₂ triplet states by O, O₂, and N₂ are adopted from Morrill and Benesch (1996) and by CO₂ and CO are taken from Dreyer et al. (1974).

Figure 3 shows the population of different vibrational levels of triplet states of N₂ at 150 km relative to the ground state. The relative vibrational popu-

lation of the $N_2(A)$ state at 130 km is also shown in Figure 3. Our calculated relative vibrational populations agree well with the calculations of Morrill and Benesch (1996) and Cartwright (1978). To show the effect of quenching, the relative vibrational populations of the $N_2(A)$ state calculated without quenching at 130 and 150 km are also shown in Figure 3. It is clear from Figure 3 that quenching does affect the vibrational population of $N_2(A)$ state at lower altitudes, mainly for vibrational levels ≤ 12 ; however, as the altitude increases the effect of quenching decreases. Figure 4 shows the steady state fractional population altitude profile of a few vibrational levels of the $A^3\Sigma_u^+$ excited state of N_2 , while Figure 5 shows them for $\nu' = 0$ level of the B , C , W , and B' states for both solar minimum and maximum conditions. At low solar activity, the vibrational populations show a peak at ~ 150 km, while during high solar activity, a broad peak ~ 140 – 160 km is seen. The quenching reduces the population by a factor of 2 to 3 around the peak, and its effect is felt up to an altitude of ~ 200 km.

After calculating the steady state density of different vibrational levels of excited triplet states of N_2 , the volume emission rate $V_{\nu'\nu''}^{\alpha\beta}$ of a vibration band $\nu' \rightarrow \nu''$ can be obtained using

$$V_{\nu'\nu''}^{\alpha\beta} = n_{\nu'}^{\alpha} \times A_{\nu'\nu''}^{\alpha\beta} \quad (\text{cm}^{-3} \text{ s}^{-1}) \quad (6)$$

where $n_{\nu'}^{\alpha}$ is the density of vibrational level ν' of state α , and $A_{\nu'\nu''}^{\alpha\beta}$ is the transition probability (s^{-1}) for the transition from the ν' level of state α to the ν'' level of state β .

Volume emission rates are height-integrated to calculate the overhead intensities. Table 1 shows the total overhead intensity for triplet transitions of N_2 during low and high solar activity at $\text{SZA}=60^\circ$ calculated by adding all the band emissions. Table 2 shows the nadir intensity ($\text{SZA}=60^\circ$) during solar minimum and maximum conditions for the prominent VK bands of N_2 ; for other triplet emissions (viz., First Positive, Second Positive, and Wu-Benesch) overhead intensities are given in Table 3. The increase in the VK band intensity from solar minimum to maximum is ~ 60 – 70% . The strongest VK band emissions (0, 5), (0, 6), (0, 7), (0, 8), (1, 9), and (1, 10) have intensities of 94 (160), 120 (204), 114 (194), 94 (155), and 88 (145) R, respectively, during solar minimum (maximum) condition. On Mars the SPICAM aboard Mars Express has recently detected VK (0, 5), (0, 6), and (0, 7) bands (Leblanc et al., 2006, 2007).

The calculated band emission rate can be inte-

grated along the line of sight at a projected distance from the centre of Venus to obtain limb profiles. Figure 6 shows the limb profiles of VK (0, 6) band at SZA of 0° and 60° for solar minimum and maximum conditions. In the case of solar minimum, the limb profile peaks at 133 (136) km for $\text{SZA}=0^\circ$ (60°), with a value of ~ 10 (~ 5) kR. During high solar activity, peak value of ~ 20 (~ 10) kR in the profiles occurs at 131 (134 km) for $\text{SZA}=0^\circ$ (60°). Thus, the intensity increases by a factor of 2 at the peak for a low to high solar activity change. The effect of the SZA is observed at lower altitudes (< 160 km) only. Above 150 km the shape of the limb profile in minimum and maximum condition are different, which is due to the difference in the Venus model atmosphere in the two solar conditions. The limb intensities of the VK (0, 4), (0, 5), and (0, 7) bands are also calculated in the model. The shape of the limb profiles of the VK (0, 4), (0, 5), and (0, 7) bands are similar to that of the VK (0, 6) band shown in Figure 6, but their limb intensity at the peak is around 44, 78, and 95%, respectively, of the limb intensity of the VK (0, 6) band.

On Mars, the SPICAM has observed limb profiles of (0, 5) and (0, 6) bands of VK emissions, since they are the strong emissions below 3000 \AA (see Table 2). The peak intensity of VK (0, 6) band on Mars is ~ 0.5 kR (Leblanc et al., 2007; Jain and Bhardwaj, 2011). This value is more than a factor of 10 lower than that calculated on Venus during low solar activity. Only a factor of 5 difference in intensity is expected due to the difference in heliocentric distances of Mars and Venus. A much larger difference is due to the higher N_2 density around the peak on Venus (138 km, $8 \times 10^9 \text{ cm}^{-3}$) compared to that on Mars (126 km, $1.5 \times 10^9 \text{ cm}^{-3}$); the N_2/CO_2 ratio being 0.12 on Venus and 0.03 on Mars at the intensity peak. However, at higher altitudes the density of N_2 on Mars is larger compared to that on Venus; *e.g.*, at 200 km, the N_2 density at Mars and Venus is 7.5×10^6 and $2.4 \times 10^6 \text{ cm}^{-3}$, respectively.

Jain and Bhardwaj (2011) have made a detailed study about the effect of electron impact cross sections of N_2 on the calculated VK band intensities on Mars. Their study suggests that the use of different electron impact cross sections can change the calculated VK band intensities up to 50%. The effect of using e- N_2 cross sections of Johnson et al. (2005) on the calculated overhead intensities of total VK, First Positive, Second Positive, and Wu-Benesch bands on Venus is shown in Table 1; intensities are smaller due to the lower cross sections of Johnson et al. (2005).

In their study Jain and Bhardwaj (2011) found that use of SOLAR2000 model of Tobiska et al. (2000),

instead of EUVAC model of Richards et al. (1994) as the solar EUV input flux in the model can increase the calculated intensities of N₂ VK bands by ~15% on Mars. A similar effect is found on Venus if the SOLAR2000 model of Tobiska et al. (2000) is used.

We have also calculated intensities for triplet transitions by taking the model atmosphere as used in Fox and Dalgarno (1981) for low solar activity at SZA = 45°. Our calculated intensities for the VK bands are about 30% higher (similar results have been seen in the case of Mars also; cf. Jain and Bhardwaj, 2011) than those of Fox and Dalgarno (1981), except for the VK (0, 2) band, which is a factor of ~8 lower than the value of Fox and Dalgarno (1981). Similar difference has been observed in the overhead intensity of VK (0, 2) band on Mars (Jain and Bhardwaj, 2011). The factor which controls the intensity of VK (0, 2) band is the transition probability for that band whose value is 3.54×10^{-3} in our model, taken from Gilmore et al. (1992). Piper (1993) has also reported similar value for the VK (0, 2) band transition probability ($\sim 4.0 \times 10^{-3}$).

Differences between our and Fox and Dalgarno (1981) calculated overhead intensities of First Positive bands ($B \rightarrow A$) are between 10 to 50%; but for a few bands, *e.g.*, (2, 0), (2, 1), (3, 1), (4, 2), and (5, 3), our calculated intensities are a factor of 2 to 4 higher. For Second Positive bands ($C \rightarrow B$) our values for transitions from 0 level of C state, are ~50% higher than the values of Fox and Dalgarno (1981) but for transitions from level 1, our values are ~30% smaller than Fox and Dalgarno values. For Wu-Benesch ($W - B$) band our calculated values are smaller than those of Fox and Dalgarno (1981) by factor of 2 to 4. These differences are mainly due to updated transition probabilities used in our model which we have taken from Gilmore et al. (1992). Piper (1993) has reported the transition probabilities of the VK bands, which are consistent with those of Gilmore et al. (1992).

5 Summary

A model for N₂ triplet bands dayglow emissions on Venus has been developed for solar minimum and maximum conditions. The Analytical Yield Spectra technique is used to calculate the steady state photoelectron flux, which is in good agreement with the Pioneer Venus Orbiter-observed electron flux. Profiles of volume excitation rates of N₂ VK bands and other triplet states are calculated using photoelectron flux. Population of any given level of triplet states has been calculated considering direct electron im-

pact excitation and quenching as well as cascading from higher triplet states in statistical equilibrium conditions. The relative vibrational populations of different triplet states have been calculated and shown in Figure 3. Overhead intensities of Vegard-Kaplan, First Positive, Second Positive, Wu-Benesch, $B' \rightarrow B$, $E \rightarrow C$, $E \rightarrow B$, $E \rightarrow A$, and Reverse First Positive bands of N₂ have been calculated and presented in Table 1. The height-integrated overhead intensities of prominent transitions in VK, First Positive, Second Positive, and $W \rightarrow B$ bands have been calculated and are given in Tables 2 and 3. We have presented the calculated limb profiles of the VK (0, 6) band for solar minimum and maximum conditions in Figure 6. Maximum change in VK bands intensity are ~50% due to changes in the N₂ triplet states electron impact excitation cross sections. An increase of ~15% in the calculated intensities is observed when the SOLAR2000 solar EUV flux model of Tobiska et al. (2000) is used instead of the EUVAC model of Richards et al. (1994). The calculated intensities of VK bands on Venus are an order of magnitude larger than those on Mars. Hence, the intensities are quite large and can be detected by the SPICAV experiment on board the Venus Express mission. However, very bright sunlit limb due to solar scattering background makes it difficult to observe N₂ VK bands in Venus dayglow by SPICAV. The relative population of vibrational levels is almost constant above 180 km on Venus, while on Mars they attain a constant value above 250 km.

References

- Avakyan, S. V., Il'in, R. N., Lavrov, V. M., Ogurtsov, G. N., 1998. In: Avakyan, S. V. (Ed.), *Collision Processes and Excitation of UV Emission from Planetary Atmospheric Gases: A Handbook of Cross Sections*. Gordon and Breach science publishers.
- Bhardwaj, A., 1999. On the role of solar EUV, photoelectrons, and auroral electrons in the chemistry of C(¹D) and the production of CI 1931 Å in the inner cometary coma: A case for comet P/Halley. *J. Geophys. Res.* 104, 1929 – 1942. doi: 10.1029/1998JE900004.
- Bhardwaj, A., 2003. On the solar EUV deposition in the inner comae of comets with large gas production rates. *Geophys. Res. Lett.* 30 (24), 2244. doi: 10.1029/2003GL018495.

- Bhardwaj, A., Haider, S. A., Singhal, R. P., 1990. Auroral and photoelectron fluxes in cometary ionospheres. *Icarus* 85, 216 – 228. doi:10.1016/0019-1035(90)90112-M.
- Bhardwaj, A., Jain, S. K., 2009. Monte Carlo model of electron energy degradation in a CO₂ atmosphere. *J. Geophys. Res.* 114. doi:10.1029/2009JA014298.
- Bhardwaj, A., Michael, M., 1999. Monte Carlo model for electron degradation in SO₂ gas: cross sections, yield spectra and efficiencies. *J. Geophys. Res.* 104 (10), 24713 – 24728. doi:10.1029/1999JA900283.
- Broadfoot, A., Hatfield, D., Anderson, E., Stone, T., Sandel, B., Gardner, J., Murad, E., Knecht, D., Pike, C., Viereck, R., 1997. N₂ triplet band systems and atomic oxygen in the dayglow. *J. Geophys. Res.* 102 (A6), 11567 – 11584. doi:10.1029/97JA00771.
- Cartwright, D., Trajmar, S., Williams, W., 1971. Vibrational Population of the $A^3\Sigma_u^+$ and $B^3\Pi_g$ States of N₂ in Normal Auroras. *J. Geophys. Res.* 76 (34), 8368 – 8377. doi:10.1029/JA076i034p08368.
- Cartwright, D. C., 1978. Vibrational populations of the excited state of N₂ under auroral condition. *J. Geophys. Res.* 83 (A2), 517 – 321. doi:10.1029/JA083iA02p00517.
- Daniell, R., Strickland, D., 1986. Dependence of Auroral Middle UV Emissions on the Incident Electron Spectrum and Neutral Atmosphere. *J. Geophys. Res.* 91 (A1), 321 – 327. doi:10.1029/JA091iA01p00321.
- Dreyer, J. W., Perner, D., Roy, C. R., 1974. Rate constants for the quenching of N₂ ($A^3\Sigma_u^+$, $\nu_A = 0 - 8$) by CO, CO₂, NH₃, NO, and O₂. *J. Chem. Phys.* 61 (8), 3164 – 3169. doi:10.1063/1.1682472.
- Feldman, P. D., Burgh, E. B., Durrance, S. T., David- sen, A. F., 2000. Far-ultraviolet spectroscopy of Venus and Mars at 4Å resolution with the Hopkins Ultraviolet Telescope on Astro-2. *Astrophys J.* 538, 395 – 400. doi:10.1086/309125.
- Fox, J. L., Bougher, S. W., 1991. Structure, luminosity, and dynamics of the Venus thermosphere. *Space Science Reviews* 55, 357 – 489. doi:10.1007/BF00177141.
- Fox, J. L., Dalgarno, A., 1981. Ionization, Luminosity and Heating of Upper atmosphere of Venus. *J. Geophys. Res.* 86, 629 – 639. doi:10.1029/JA086iA02p00629.
- Gérard, J.-C., Cox, C., Saglam, A., Bertaux, J.-L., Villard, E., Nehmé, C., 2008. Limb observations of the ultraviolet nitric oxide nightglow with SPICAV on board Venus Express. *J. Geophys. Res.* 113. doi:10.1029/2008JE003078.
- Gérard, J.-C., Hubert, B., Gustin, J., Shematovich, V. I., Bisikalo, D., Gladstone, G. R., Esposito, L. W., 2011. EUV spectroscopy of the Venus dayglow with UVIS on Cassini. *Icarus* 211 (1), 70 – 80. doi:10.1016/j.icarus.2010.09.020.
- Gilmore, F. R., Laher, R. R., Espy, P. J., 1992. Franck-Condon factors, r-centroids, electronic transition moments, and Einstein coefficients for many nitrogen and oxygen band systems. *J. Phys. Chem. Ref. Data* 21, 1005 – 1107. doi:10.1063/1.555910.
- Gronoff, G., Lilensten, J., Simon, C., Barthélemy, M., Leblanc, F., Dutuit, O., 2008. Modelling the Venusian airglow. *Astronomy and Astrophysics* 482 (3), 1015 – 1029. doi:10.1051/0004-6361:20077503.
- Hedin, A. E., Niemann, H. B., Kasprzak, W. T., Seiff, A., 1983. Global Empirical Model of The Venus Thermosphere. *J. Geophys. Res.* 88 (A1), 73 – 83. doi:10.1029/JA088iA01p00073.
- Hubert, B., Gérard, J. C., Gustin, J., Shematovich, V. I., Bisikalo, D. V., Stewart, A. I., Gladstone, G. R., 2010. UVIS observations of the FUV OI and CO 4P Venus dayglow during the Cassini flyby. *Icarus* 207 (2), 549 – 557. doi:10.1016/j.icarus.2009.12.029.
- Itikawa, Y., 2006. Cross sections for electron collisions with nitrogen molecules. *J. Phys. Chem. Ref. Data* 35 (1), 31 – 53. doi:10.1063/1.1937426.
- Jackman, C., Garvey, R., Green, A., 1977. Electron impact on atmospheric gases, I. Updated cross sections. *J. Geophys. Res.* 82 (32), 5081 – 5090. doi:10.1029/JA082i032p05081.
- Jain, S. K., Bhardwaj, A., 2011. Model calculation of N₂ Vegard-Kaplan band emissions in Martian dayglow. *J. Geophys. Res.* 116, E07005. doi:10.1029/2010JE003778.
- Johnson, P. V., Malone, C. P., Kanik, I., Tran, K., Khakoo, M. A., 2005. Integral cross sections for the direct excitation of the $A^3\Sigma_u^+$, $B^3\Pi_g$, $W^3\Delta_u$, $B^3\Sigma_u^-$, $a^1\Sigma_u^-$, $a^1\Pi_g$, $w^1\Delta_u$, and $C^3\Pi_u$ electronic states in

- N_2 by electron impact. *J. Geophys. Res.* 110. doi:10.1029/2005JA011295.
- Leblanc, F., Chaufray, J. Y., Bertaux, J. L., 2007. On Martian nitrogen dayglow emission observed by SPICAM UV spectrograph/Mars Express. *Geophys. Res. Lett.* 34. doi:10.1029/2006GL0284.
- Leblanc, F., Chaufray, J. Y., Lilensten, J., Witasse, O., Bertaux, J.-L., 2006. Martian dayglow as seen by the SPICAM UV spectrograph on Mars Express. *J. Geophys. Res.* 111. doi:10.1029/2005JE002664.
- Michael, M., Bhardwaj, A., 1997. On the dissociative ionization of SO_2 in the Io's atmosphere. *Geophys. Res. Lett.* 24, 1971 – 1974. doi:10.1029/97GL02056.
- Morrill, J., Benesch, W., 1996. Auroral N_2 emissions and the effect of collisional processes on N_2 triplet state vibrational populations. *J. Geophys. Res.* 101 (A1), 261 – 274. doi:10.1029/95JA02835.
- Paxton, L. J., Anderson, D. E., 1992. Far ultraviolet remote sensing of Venus and Mars. *AGU Geophysical Monograph Series.* 66, 113 – 189.
- Piper, L. G., 1993. Reevaluation of the transition-moment function and Einstein coefficients for the N_2 ($A^3\Sigma_u^+ - X^1\Sigma_g$) transition. *J. Chem. Phys.* 75, 3174 – 3181. doi:10.1063/1.465178.
- Richards, P. G., Fennelly, J. A., Torr, D. G., 1994. EUVAC: A solar EUV flux model for aeronomic calculations. *J. Geophys. Res.* 99, 8981 – 8992. doi:10.1029/94JA00518.
- Schunk, R. W., Nagy, A. F., 2000. *Ionospheres: Physics, Plasma Physics, and Chemistry.* Cambridge University Press.
- Sharp, W. E., 1971. Rocket-borne spectroscopic measurements in the ultraviolet aurora: Nitrogen Vegard-Kaplan bands. *J. Geophys. Res.* 76 (04), 987 – 1005. doi:10.1029/JA076i004p00987.
- Singhal, R. P., Bhardwaj, A., 1991. Monte Carlo simulation of photoelectron energization in parallel electric fields: Electroglow on Uranus. *J. Geophys. Res.* 96, 15963 – 15972. doi:10.1029/90JA02749.
- Singhal, R. P., Jackman, C., Green, A. E. S., 1980. Spatial aspects of low and medium energy electron degradation in N_2 . *J. Geophys. Res.* 85 (A3), 1246 – 1254. doi:10.1029/JA085iA03p01246.
- Spenner, K., Dóbbé, Z., Nagy, A. F., Knudsen, W. C., Lotze, W., 1997. Photoelectron fluxes in the Venus dayside ionosphere. *J. Geophys. Res.* 102 (A2), 2577 – 2583. doi:10.1029/96JA03341.
- Tobiska, W. K., Woods, T., Eparvier, F., Viereck, R., Floyd, L., Bouwer, D., Rottman, G., White, O. R., 2000. The SOLAR2000 empirical solar irradiance model and forecast tool. *J. Atmos. Sol. Terr. Phys.* 62, 1233 – 1250. doi:10.1016/S1364-6826(00)00070-5.

Table 1: Height-integrated overhead intensities of triplet transitions of N₂.

Band	Intensity (kR)	
	Min [*]	Max. [†]
Vegard-Kaplan ($A \rightarrow X$)	1.9 (1.5)	3.2
First Positive ($B \rightarrow A$)	3 (2.0)	6
Second Positive ($C \rightarrow B$)	0.4 (0.1)	0.8
Wu-Benesch ($W \rightarrow B$)	0.5 (0.4)	1.1
$B' \rightarrow B$	0.2 (0.08)	0.5
$E \rightarrow A$	3E-3 (3E-3) [‡]	7E-3
$E \rightarrow B$	5E-4 (5E-4)	1E-3
$E \rightarrow C$	2E-3 (2E-3)	4E-3
R1P [§] ($A \rightarrow B$)	0.5 (0.4)	0.9

^{*}Solar minimum (F10.7=80). Values in the bracket is for e-N₂ cross sections taken from [Johnson et al. \(2005\)](#).

[†]Solar maximum (F10.7=200).

[‡]3E-3 = 3×10^{-3} .

[§]Reverse First Positive.

Table 2: N₂ Vegard-Kaplan Band ($A^3\Sigma_u^+ \rightarrow X^1\Sigma_g^+$) height-integrated overhead intensity.

Band $\nu' - \nu''$	Band Origin	Overhead Intensity (R)	
		Min.*	Max.†
0-2	2216	4	7
0-3	2334	20	34
0-4	2463	53	91
0-5	2605	94	160
0-6	2762	120	204
0-7	2937	114	194
0-8	3133	84	143
0-9	3354	49	84
1-3	2258	16	27
1-4	2379	24	40
1-8	2998	63	105
1-9	3200	94	155
1-10	3427	88	145
1-11	3685	59	97
1-12	3980	30	49
1-13	4321	12	19
2-10	3270	26	41
2-11	3503	54	86
2-12	3769	58	93
2-13	4074	41	66
3-12	3583	15	24
3-13	3857	37	60
3-14	4171	41	67
4-11	3198	16	26
4-15	4274	25	41
4-16	4650	26	42
5-17	4771	18	29
5-18	5229	16	26
6-19	5372	13	21
7-0	1689	11	18
8-0	1655	12	20
9-0	1622	9	16

*Solar minimum condition.

†Solar maximum condition.

Table 3: Calculated height-integrated overhead intensity of N₂ triplet emissions.

Band ($\nu' - \nu''$)	Band Origin Å	Intensity (R)		Band ($\nu' - \nu''$)	Band Origin Å	Intensity (R)	
		Min.*	Max.†			Min.*	Max.†
First Positive $B^3\Pi_g - A^3\Sigma_u^+$				Reverse first positive ($A^3\Sigma_u^+ - B^3\Pi_g$)			
0-0	10469	229	465	9-0	42700	29	51
0-1	12317	123	250	10-1	55100	45	84
0-2	14895	37	75	Herman-Kaplan ($E^3\Sigma_g^+ - A^3\Sigma_u^+$)			
1-0	8883	367	744	0-1	2243	0.35	0.8
1-2	11878	68	138	0-2	2316	0.57	1.3
1-3	14201	52	105	0-3	2392	0.63	1.4
2-0	7732	182	372	0-4	2472	0.52	1.2
2-1	8695	236	480	$E^3\Sigma_g^+ - B^3\Pi_g$			
2-2	9905	44	89	0-1	2877	0.14	0.3
2-4	13572	33	68	0-2	3181	0.11	0.3
3-1	7606	252	515	$E^3\Sigma_g^+ - C^3\Pi_u$			
3-2	8516	66	135	0-0	14713	1.7	3.8
3-3	9648	79	162	0-1	20824	0.14	0.3
4-1	6772	77	158	$B'^3\Sigma_u^- - B^3\Pi_g$			
4-2	7484	193	395	3-1	10816	5.4	11.2
4-4	9404	58	119	4-1	9375	6.3	13
5-2	6689	87	178	4-2	8990	5.8	12.2
5-3	7368	103	211	5-2	9626	9.1	19
6-3	6608	71	145	6-2	8501	8	16.9
7-4	6530	47	96	6-3	9886	8.7	18.2
Wu-Benesch ($W^3\Delta_u - B^3\Pi_g$)				8-4	8947	8.6	18
2-0	33206	16	34	9-4	8011	7.5	15.6
3-0	22505	14	29	9-5	9180	6.3	13
3-1	36522	12	25	10-4	7264	4.8	10.1
4-1	24124	21	43	10-5	8213	6.5	13.6
5-1	18090	19	40	Second Positive $C^3\Pi_u - B^3\Pi_g$			
5-2	25962	18	38	0-0	3370	137	291
6-2	19193	23	49	0-1	3576	92	196
7-2	15281	19	39	0-2	3804	37	79
7-3	20421	21	43	1-0	3158	35	75
8-3	16112	21	43	1-2	3536	16	35
9-3	13347	15	31				
9-4	17024	18	37				
10-4	14014	15	31				
10-5	18030	12.5	26				

*Solar minimum condition.

†Solar maximum condition.

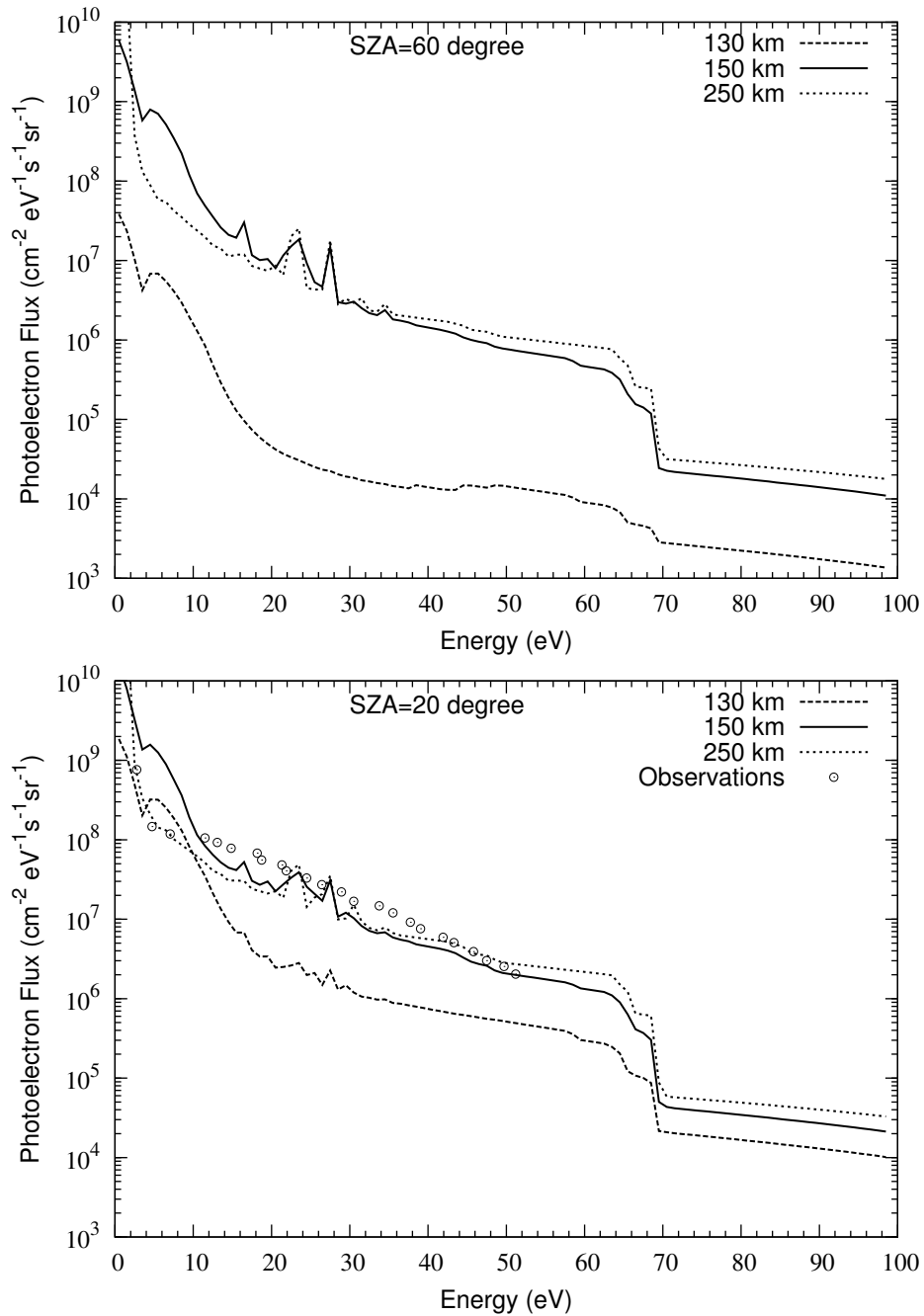


Figure 1: Model calculated photoelectron flux for low (upper panel) and high (bottom panel) solar activity conditions at 130, 150, and 230 km. Symbols in bottom panel represent the Pioneer Venus Orbiter-observed values averaged over 206-296 km and 8° - 35° SZA, taken from [Spenner et al. \(1997\)](#).

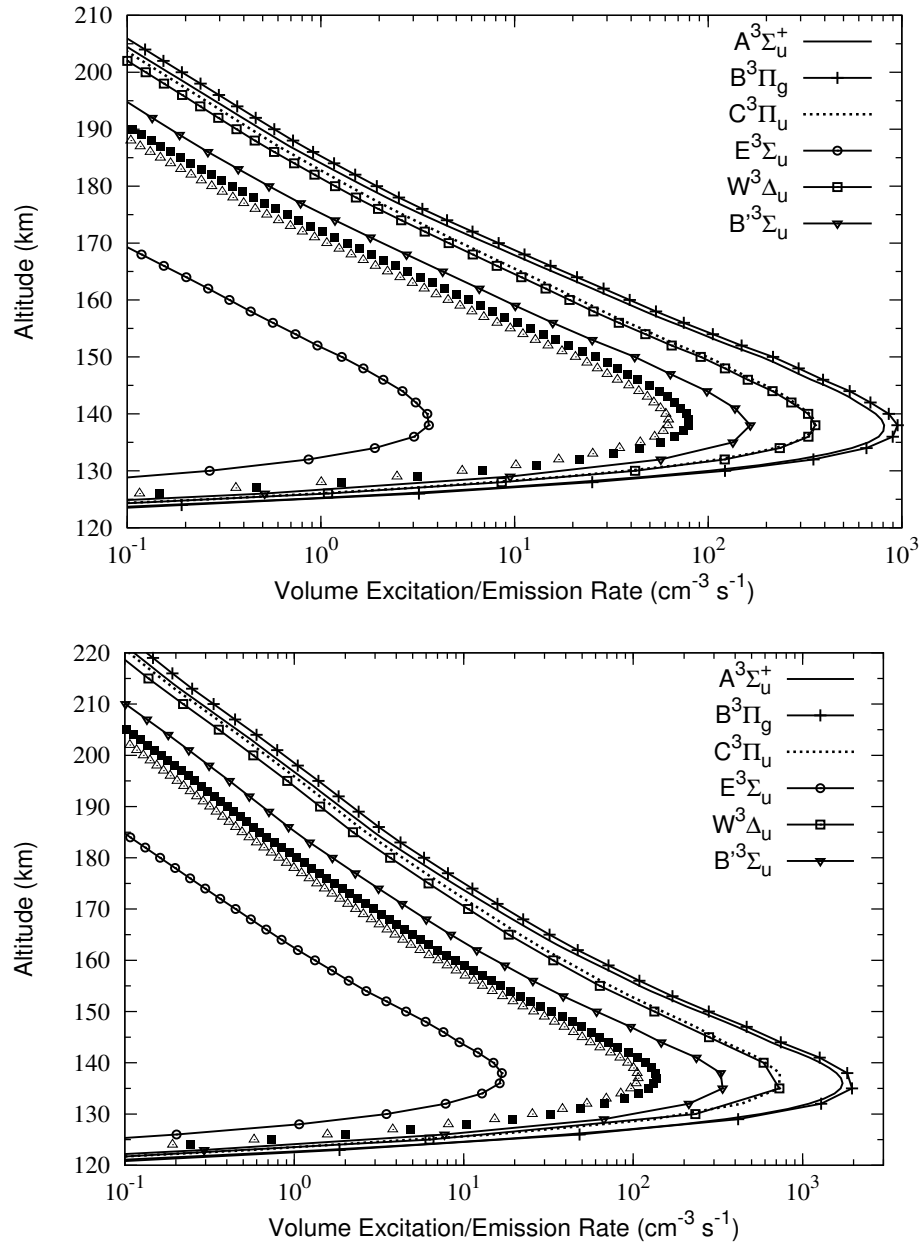


Figure 2: Volume excitation rates of various triplet states of N_2 by direct electron impact excitation in solar minimum (upper panel) and maximum (bottom panel) conditions at $SZA = 60^\circ$. The rate of $E^3\Sigma_u$ state is plotted after multiplying by 2. Solid square and open triangle represent the volume emission rates of the VK (0, 6) and VK (0, 5) bands, respectively.

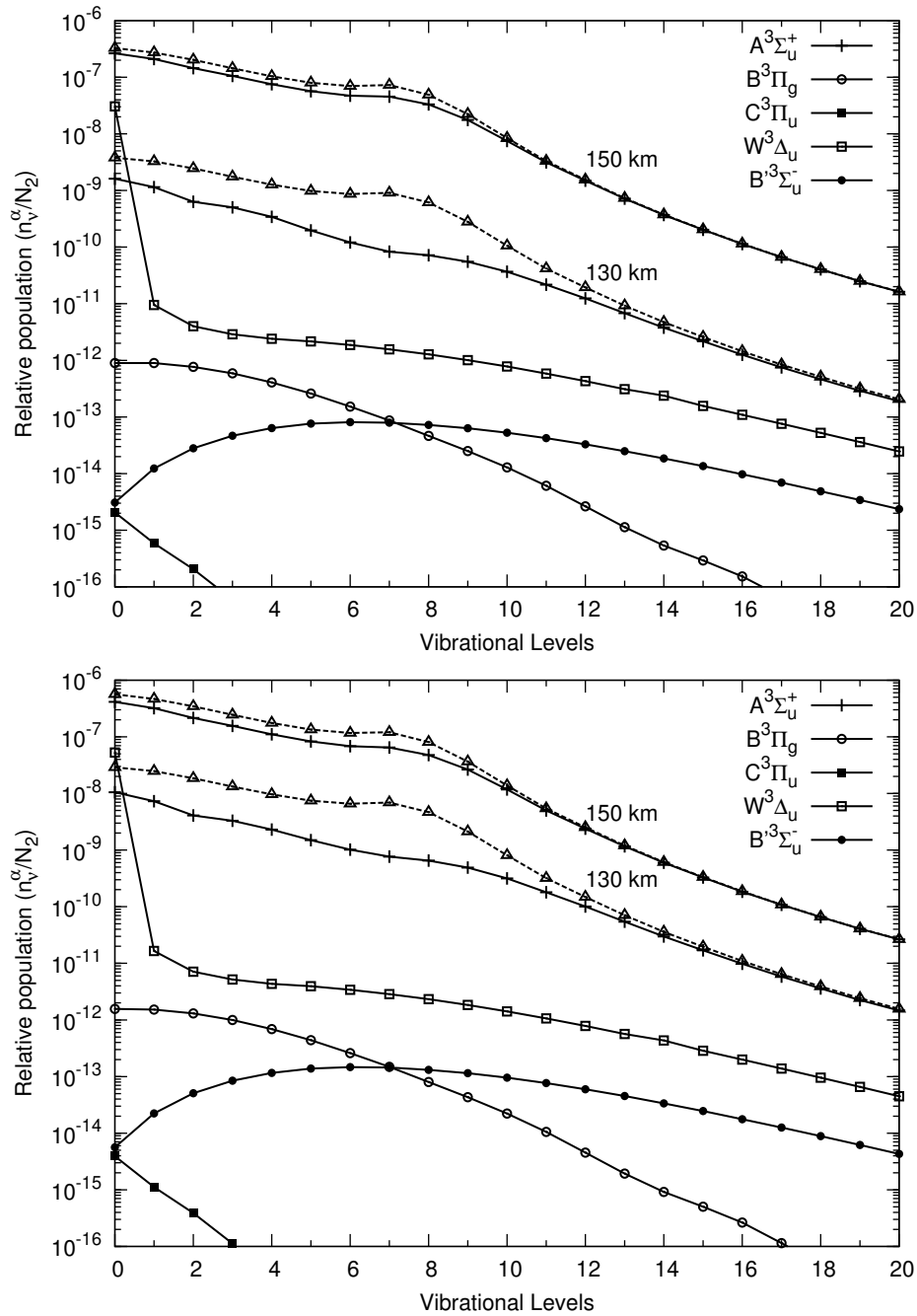


Figure 3: Relative population of vibrational levels of different triplet state of N_2 with respect to $N_2(X)$ at 150 km for low (upper panel) and high (bottom panel) solar activities, at $SZA=60^\circ$. Dashed line with triangle shows the relative vibrational population of $A^3\Sigma_u^+$ without quenching at 130 and 150 km.

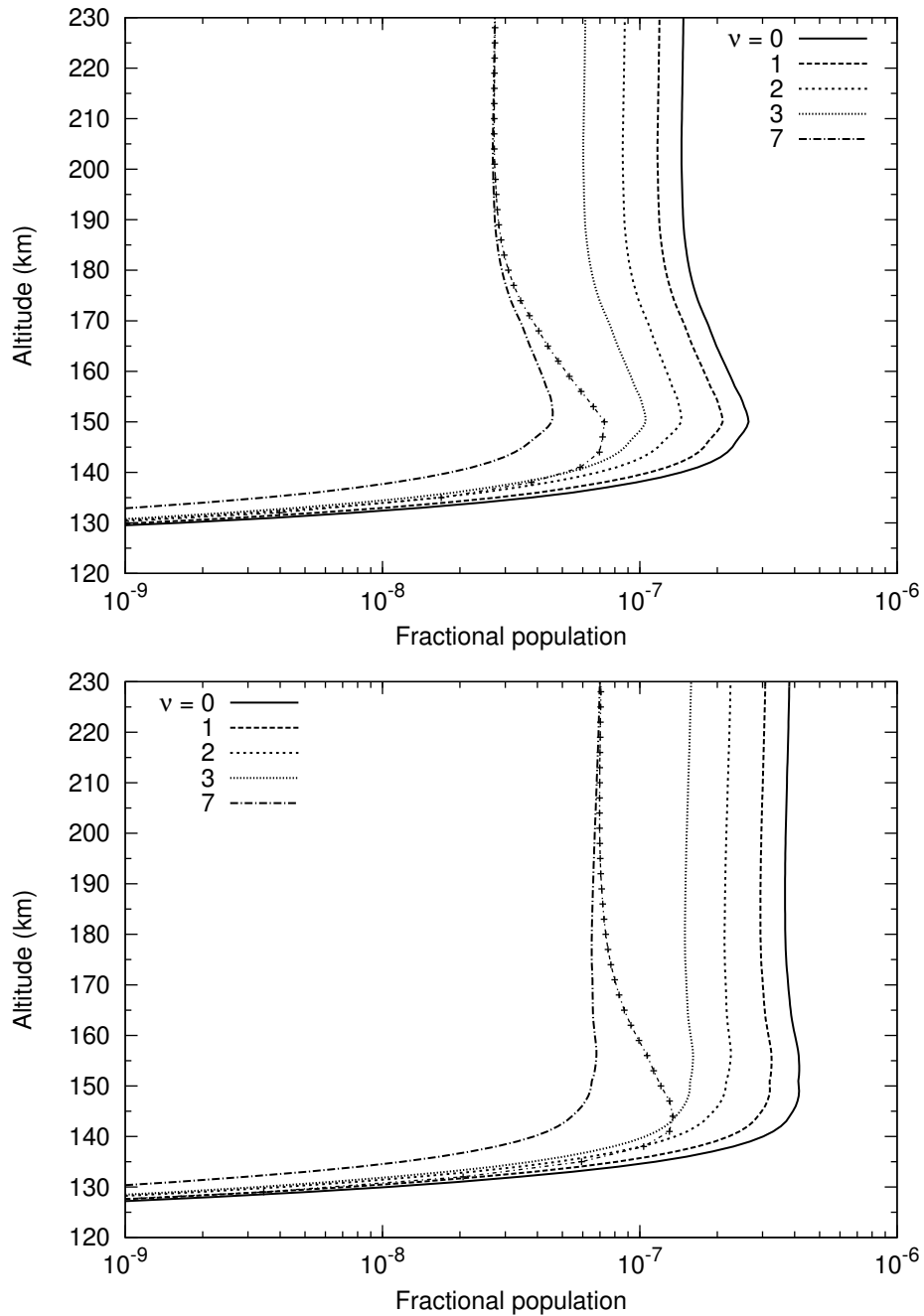


Figure 4: Altitude profiles of relative population of selected vibrational levels of the $N_2(A)$ state with respect to the $N_2(X)$ for low (upper panel) and high (bottom panel) solar activities, at $SZA=60^\circ$. Dashed line with symbols shows the relative population of vibrational level 7 without quenching.

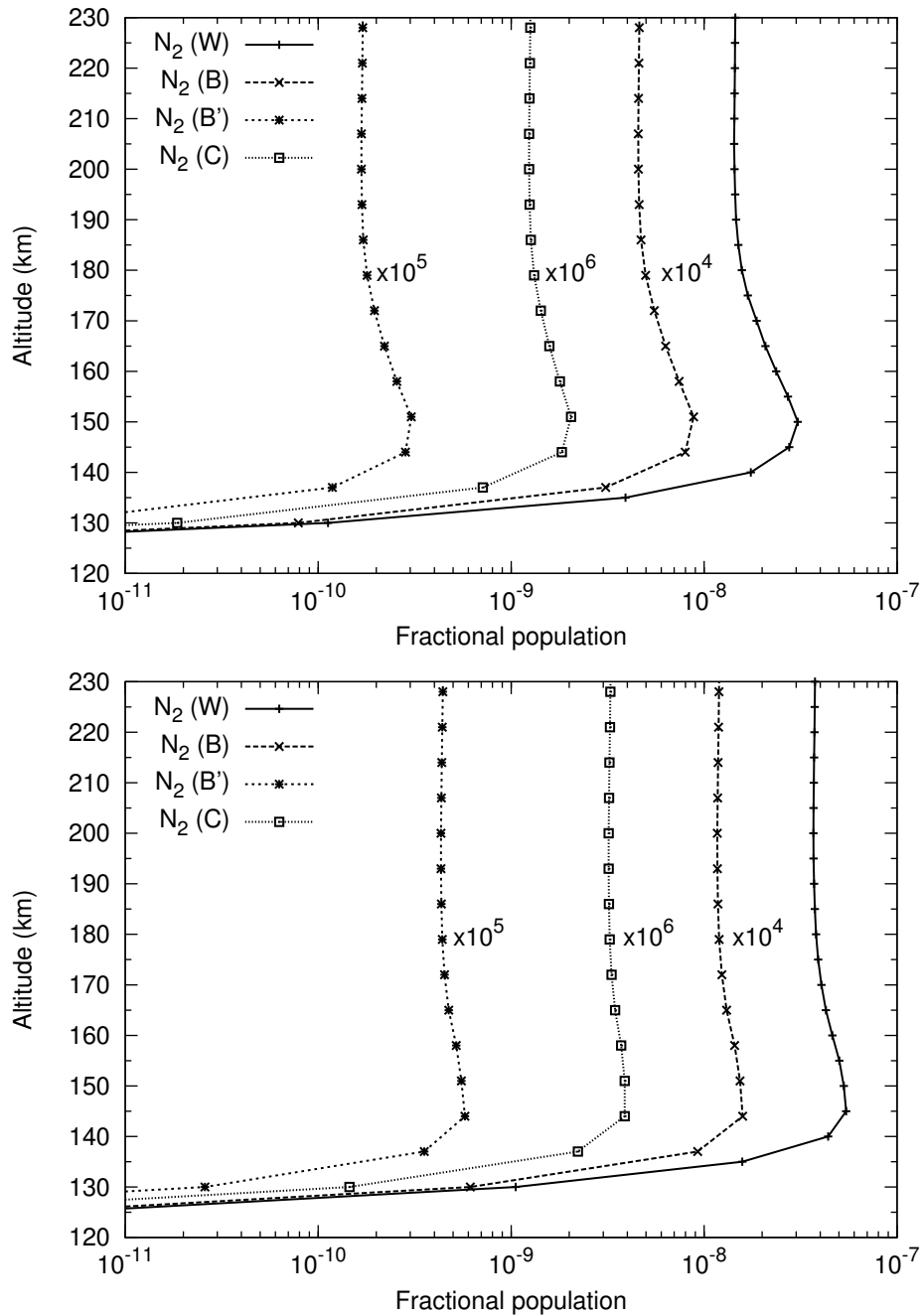


Figure 5: Altitude profiles of relative population of 0 vibrational level of B , B' , C , and W states of N_2 with respect to the $N_2(X)$ for low (upper panel) and high (bottom panel) solar activities, at $SZA=60^\circ$. Populations of B , B' , and C have been plotted after multiplying by a factor of 10^4 , 10^5 , and 10^6 , respectively.

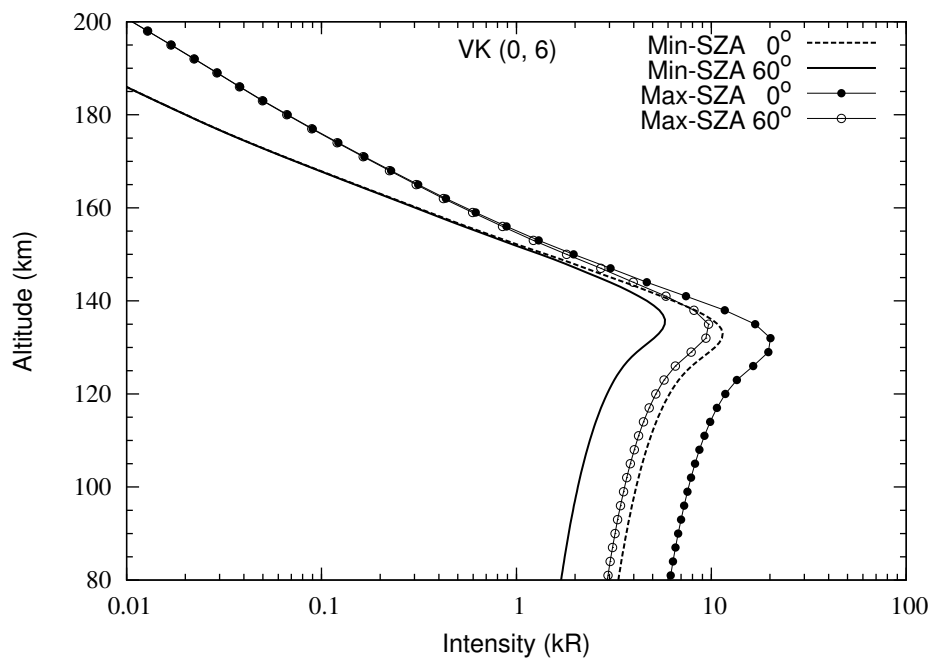


Figure 6: Calculated limb intensity of VK (0, 6) band for low (min) and high (max) solar activity conditions, at SZA of 0° and 60°.